

IMPLEMENTATION OF HIGH-ORDER COMPACT SCHEMES TO THE ITERATIVE PARABOLIZED NAVIER-STOKES EQUATIONS

Vahid Esfahanian* , Kazem Hejranfar** , Hossein Mahmoodi Darian***

*Associate Professor, Mechanical Engineering Dept., University of Tehran, Iran,

**Assistant Professor, Aerospace Engineering Dept., Sharif University of Technology, Iran,

***Ph.D. Candidate Mechanical Engineering Dept., University of Tehran, Iran

Keywords: *Compact Finite Difference, PNS equations*

Abstract

The numerical solution of the parabolized Navier-Stokes (PNS) and globally iterated PNS (IPNS) equations for accurate computation of hypersonic axisymmetric flowfields is obtained by using the fourth-order compact finite-difference method. The PNS and IPNS equations in the general curvilinear coordinates are solved by using the implicit finite-difference algorithm of Beam and Warming type with a high-order compact accuracy. A shock fitting procedure is utilized in both the compact PNS and IPNS schemes to obtain accurate solutions in the vicinity of the shock. The main advantage of the present formulation is that the basic flow variables and their first and second derivatives are simultaneously computed with the fourth-order accuracy. The computations are performed for a benchmark case; hypersonic axisymmetric flow over a blunt cone at Mach 8. The present results for the flowfield variables and also their derivatives are compared with those of the second-order method and accuracy analysis is performed to insure the fourth-order accuracy of the proposed method. A sensitivity study is performed for the basic flowfield, including profiles and their derivatives obtained from the fourth-order compact PNS and IPNS solutions, and the effects of grid size and numerical dissipation term used are discussed. The present work represents the first

known application of a high-order compact finite-difference method to the PNS schemes which are computationally more efficient than Navier-Stokes solutions.

1 Introduction

Due to high sensitivity of some problems such as flow stability analysis to very small disturbances in basic flow variables, using high accuracy numerical methods for solving basic flow variables is essential. Traditional high accuracy finite-difference methods use larger stencil sizes which make boundary treatment difficult. Moreover, spectral methods are restricted to special grids, whereas compact methods are capable of producing higher order accuracies without any increase in numerical stencil. Compared with the traditional finite-difference schemes of the same order of accuracy, compact schemes have been proved to be significantly more accurate with the added benefit of using smaller stencil sizes, which can be essential when treating non-periodic boundary conditions [1, 2].

The objective of the present work is to implement a fourth-order compact finite-difference method to the parabolized Navier-Stokes equations for accurate computation of hypersonic flows. The study has been shown that the PNS schemes can be used for an efficient and fast computing the basic flow and the associated flow stability results in hypersonic speeds [3, 4]. It

was also found that the stability results are more sensitive to the accuracy of the basic flowfield and the derivatives of the flow variables [3]-[5]. Therefore, by implementation of the high-order compact finite-difference method to the PNS schemes [6, 7], accurate basic flow models suitable for the stability analysis and transition prediction of hypersonic flows are efficiently provided.

In the present work, the high-order accurate solution of hypersonic axisymmetric flows is obtained by implementing a fourth-order compact finite-difference method based on an implicit algorithm to both the PNS and globally iterated PNS (IPNS) equations. A shock fitting procedure is used in both the PNS and IPNS compact schemes to obtain accurate solutions in the vicinity of the shock. The main advantage of the present formulation is that the basic flow profiles and their first and second derivatives, required for the flow stability analysis, are automatically computed with the fourth-order accuracy. At first, the dispersive and dissipative properties of the compact methods are discussed. Then, the fourth-order compact method is implemented to the quasi one-dimensional Euler equations to solve compressible flow inside the Shubin nozzle. Finally, The results of the fourth-order compact finite-difference method for the PNS and IPNS schemes are presented for hypersonic flow over a blunt cone at Mach 8. The present results for the basic flow variables and also their derivatives are compared with those of the second-order method and accuracy analysis is performed to insure the fourth-order accuracy of the proposed method. A sensitivity study is performed to investigate the effects of grid size and numerical dissipation term on the accuracy of basic flow variables and their derivatives.

2 Governing Equations

2.1 The PNS Equations

The Thin Layer Navier-Stokes (TLNS) equations are obtained from the full Navier-Stokes equations by neglecting viscous terms associated with

the streamwise derivatives. The PNS equations are obtained by dropping the unsteady term in the TLNS equations and modifying the streamwise pressure gradient in the streamwise momentum equation to permit stable marching. The PNS equations for axisymmetric compressible flow can be written in dimensionless and conservative form in the generalized coordinate system (ξ, η) as follows:

$$\frac{\partial \bar{F}}{\partial \xi} + \frac{\partial \bar{G}}{\partial \eta} + \bar{H} = 0 \quad (1)$$

$$\bar{F} = \bar{F}_i, \quad \bar{G} = \bar{G}_i - \bar{G}_v, \quad \bar{H} = \bar{H}_i - \bar{H}_v$$

where the solution vector is

$$\bar{U} = J^{-1} \hat{U} = J^{-1} [\rho, \rho u, \rho v, E]^T$$

and \bar{F}_i , \bar{G}_i and \bar{H}_i are the inviscid flux vectors and \bar{G}_v and \bar{H}_v are the viscous flux vectors.

The PNS equations are a mixed set of hyperbolic-parabolic equations in the marching direction, provided that the inviscid flow is supersonic, the streamwise velocity component is everywhere positive, and the streamwise pressure gradient term is either dropped in the subsonic region or the departure behavior is suppressed using a suitable technique. The presence of the streamwise pressure gradient term in the streamwise convective flux vector permits the upstream influences to occur in the subsonic region of the boundary layer, which leads to exponentially growing solutions referred to as departure solutions [8]. Stable marching of numerical solution of the PNS equations is achieved in the subsonic region of the boundary layer by using the methods proposed by Vigneron et al. [9] and Schiff and Steger [10]. For this study, the Vigneron et al. [9] technique is implemented to prevent departure solutions.

In the Vigneron et al. approximation, the streamwise pressure gradient in the momentum equations is split into an implicit contribution and an explicit contribution

$$\frac{\partial p}{\partial \xi} = \left[\omega \frac{\partial p}{\partial \xi} \right]_{\text{implicit}} + \left[(1 - \omega) \frac{\partial p}{\partial \xi} \right]_{\text{explicit}} \quad (2)$$

The weighting function ω is determined as

$$\omega = \min \left[1, \frac{\sigma \gamma M_\xi^2}{1 + (\gamma - 1) M_\xi^2} \right] \quad (3)$$

where M_ξ is the local streamwise Mach number and σ is a safety factor to account for nonlinearities in the analysis. The value of σ in the pressure correction relation should be very close to 1; otherwise undesirable oscillations appear around the sonic line especially in the pressure profile. To introduce the Vigneron et al. technique into the PNS equations, a new vector \bar{F}^* is defined as

$$\bar{F}^* = \bar{F} - \bar{P} \quad (4)$$

Thus, the new form of the PNS equations appears as

$$\frac{\partial \bar{F}^*}{\partial \xi} + \frac{\partial \bar{P}}{\partial \xi} + \frac{\partial \bar{G}}{\partial \eta} + \bar{H} = 0 \quad (5)$$

where the inviscid vectors \bar{F}^* and \bar{P} are

$$\bar{F}^* = J^{-1} \begin{pmatrix} \rho U_c \\ \rho u U_c + \omega \xi_x p \\ \rho v U_c + \omega \xi_y p \\ (E + p) U_c \end{pmatrix},$$

$$\bar{P} = J^{-1} \begin{pmatrix} 0 \\ (1 - \omega) \xi_x p \\ (1 - \omega) \xi_y p \\ 0 \end{pmatrix}$$

and (u, v) are the Cartesian velocity components, U_c denotes the contravariant velocity in ξ direction, $U_c = \xi_x u + \xi_y v$, ρ is the density, p is the pressure and E is the total energy per unit volume. In this study, the ratio of specific heats is assumed constant, $\gamma = 1.4$, the molecular viscosity μ is determined by the Sutherland law and the coefficient of thermal conductivity is calculated by assuming a constant Prandtl number, $Pr = 0.72$. Finally, the system of PNS equations is closed by employing the perfect-gas equations of state. The preceding equations have been nondimensionalized using the reference length L (R_N dimensional nose radius) and freestream conditions.

In the present PNS solver, the "elliptic" part of the streamwise pressure gradient term ($\partial p / \partial \xi$)

responsible for upstream disturbance propagation is omitted to permit the space-marching procedure to be stable. This term will be treated explicitly in the IPNS equations as is discussed in the next subsection.

2.2 The IPNS Equations

For solving the flowfields with significant upstream influences, the omitting of the explicit part of the streamwise pressure gradient may affect the accuracy of basic flow variables and their derivatives. In these cases, the globally iterated PNS equations, called the Reduced Navier-Stokes (RNS) equations, can be used and the upstream influences are taken into account by the forward differencing of the elliptic part of streamwise pressure gradient. The globally iterated PNS (IPNS) scheme has been used by several investigators. The IPNS model presented herein is based on the method proposed by Barnett and Davis [11]. This IPNS scheme utilizes an alternating direction explicit (ADE) procedure which is in the form of a two-step calculation procedure for each global iteration. In the ADE method, the streamwise pressure gradient is split using Vigneron's technique and a fictitious unsteady term is appended to the elliptic part as follows:

$$\frac{\partial p}{\partial \xi} = \omega \frac{\partial p}{\partial \xi} + (1 - \omega) \left[\frac{\partial p}{\partial \xi} - \frac{\partial p}{\partial t} \right] \quad (6)$$

to permit the upstream propagation of information through the subsonic region in a hyperbolic manner. Because the IPNS scheme employs the full pressure gradient term in the subsonic region of the boundary layer, it can give a solution comparable with that of the TLNS scheme [3, 4]. Thus, by implementing the fourth-order compact finite-difference method to the IPNS scheme, a high-order accurate basic flow model appropriate for the stability analysis of hypersonic flow can be efficiently provided.

2.3 Boundary Conditions and Initial Data

The boundary conditions at the wall consist of no-slip conditions for velocity components, a

specified wall-temperature or an adiabatic wall, and zero pressure gradient approximation normal to the wall. The wall for the cases studied here is assumed to be adiabatic. At the upper boundary, the bow shock is fitted using a shock fitting technique to obtain an accurate solution of the PNS equations near the shock. The advantage of the shock-fitting method over the shock-capturing method is in its capability to produce oscillation-free profiles especially in the vicinity of the strong shocks, and therefore, improve accuracy of the results.

The PNS equations are not self-starting for blunt body computations, and therefore need appropriate initial conditions. The starting data of the PNS equations is provided by the solution of the TLNS equations for the blunt cone. The TLNS equations in the nose region are solved by the second-order method with fine grid in order to have the initial data with sufficient accuracy. Figure 1 shows the initial conditions and the marching procedure for the solution of the PNS equations. The starting solution on an initial data surface where the inviscid flow is supersonic is obtained from the solution of the TLNS model.

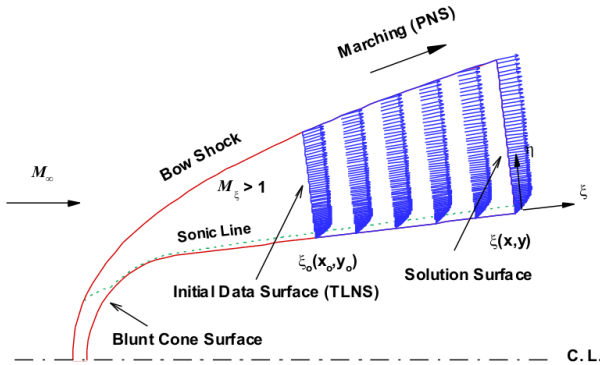


Fig. 1 Marching procedure and initial data surface for starting the PNS solution over a blunt cone. The figure also shows development of the velocity field.

2.4 Computational Grid

An algebraic grid scheme is used to compute flowfield. The lines of constant η are distributed uniformly along the body surface and are orthogonal to the body. To insure that the viscous regions are adequately resolved, the lines of constant η are clustered near the body surface according to [8].

$$\frac{x - x_w}{x_s - x_w} = \bar{a}, \quad \frac{y - y_w}{y_s - y_w} = \bar{a} \quad (7)$$

where

$$\bar{a} = 1 + \bar{\beta} \left[\frac{1 - \bar{a}^{1-\eta/\eta_{max}}}{1 + \bar{a}^{1-\eta/\eta_{max}}} \right]$$

in which the clustering parameter $\bar{\beta}$, is assigned to be 1.01 for all calculations. The above grid is used for both the PNS and IPNS equations.

3 Numerical Simulation

The numerical solution of the PNS and IPNS equations in the generalized coordinate system is obtained by using an implicit finite-difference method in the wall-normal direction η , similar to the Beam and Warming method [3, 4, 13], in which the basic flow variables and their first and second derivatives are automatically computed with the fourth-order accuracy [6, 7]. The numerical algorithm of the PNS equations for a marching step $\Delta\xi$ using the first-order backward Euler implicit scheme can be written in delta form as

$$\Delta\bar{F}^* + \Delta\xi \left[\frac{\partial\Delta\bar{G}}{\partial\eta} + \Delta\bar{H} \right]^i = -\Delta\xi \left[\frac{\partial\bar{G}}{\partial\eta} + \bar{H} \right]^i - \Delta P^i \quad (8)$$

after linearization, the equations are reduced to the following nonconservative form

$$C_0\Delta\bar{U}^i + C_1\Delta\bar{U}_\eta^i + C_2\Delta\bar{U}_{\eta\eta}^i = C_R \quad (9)$$

where $\Delta\bar{U}^i = \bar{U}^{i+1} - \bar{U}^i$ and $(\)_\eta = \partial/\partial\eta$ represents the derivative with respect to η . When the

traditional central scheme is used, the unknowns are $\Delta\bar{U}^i$ and the blocks are 4×4 and the matrix of coefficients is tridiagonal. Using a traditional fourth-order differencing does not keep this matrix tridiagonal while the present compact formulation keeps the tridiagonality of the system of equations at the expense of having 12×12 blocks. The following fourth-order compact relations for the first and second derivatives are used ($f' = \Delta\bar{U}_\eta$, $f'' = \Delta\bar{U}_{\eta\eta}$)

$$\begin{aligned} \frac{f'_{i+1} + 4f'_i + f'_{i-1}}{6} &= \frac{f_{i+1} - f_{i-1}}{2\Delta\eta} + O(\Delta\eta)^4 \\ \frac{f''_{i+1} + 10f''_i + f''_{i-1}}{12} &= \frac{f_{i+1} - 2f_i + f_{i-1}}{(\Delta\eta)^2} + O(\Delta\eta)^4 \end{aligned} \quad (10)$$

to complete the system of equations for computing the flowfield. In addition to having less truncation error of the present formulation of the compact method in comparison with the traditional fourth-order scheme, the main advantage of the present formulation is that the basic flow variables and their first and second derivatives, required for the flow stability analysis, are simultaneously computed with the fourth-order accuracy. It has been shown that the traditional finite-difference method for the discrete differentiation of the basic flow profiles causes oscillations near wall where high clustering grid points are used [3, 4]. The present formulation causes less numerical oscillations compared to the traditional method.

3.1 Numerical Dissipation Term

High-order dissipation term must be added to damp high-frequency oscillations associated with the central differencing of derivatives in the η -direction. Herein, a 6th-order dissipation term is used to stabilize the numerical instability of the method

$$D_e = \varepsilon_e \left[\frac{\partial \bar{F}^*}{\partial \bar{U}} \right] (\nabla_\eta \Delta_\eta)^3 \bar{U}^i \quad (11)$$

This term is added to the right-hand side of the Eq. (9). The stability bound for the dissipation coefficient is obtained from the stability analysis of the numerical method (see App. A). The present study demonstrates that the basic flow profiles and their derivatives based on high-order compact methods are sensitive to the grid size and especially the numerical dissipation term used in computing the flowfield, as discussed in the numerical results section.

3.2 Boundary Treatment

The no-slip conditions for the velocity components on the wall using the conservative variables are

$$\bar{U}_2^{i+1} = \bar{U}_3^{i+1} = 0$$

implies

$$\Delta\bar{U}_2^{i+1} = \Delta\bar{U}_3^{i+1} = 0 \quad (12)$$

where subscripts indicate the elements of $\Delta\bar{U}$, not the grid numbers. Also the zero pressure gradient approximation normal to the wall along with the no-slip conditions gives

$$\left. \frac{\partial p}{\partial \eta} \right|_{wall} = 0$$

which implies

$$\frac{\partial}{\partial \eta} (J\bar{U}_4)^{i+1} = 0 \quad (13)$$

or

$$\begin{aligned} J_\eta^{i+1} \Delta\bar{U}_4^i + J^{i+1} (\Delta\bar{U}_4^i)_\eta &= \\ - \left(J_\eta^{i+1} \Delta\bar{U}_4^i + J^{i+1} (\bar{U}_4^i)_\eta \right) & \end{aligned} \quad (14)$$

and the adiabatic wall with the above zero pressure gradient yields

$$\left. \frac{\partial p}{\partial \eta} \right|_{wall} = 0$$

which implies

$$\begin{aligned} J_\eta^{i+1} \Delta\bar{U}_1^i + J^{i+1} (\Delta\bar{U}_1^i)_\eta &= \\ - \left(J_\eta^{i+1} \Delta\bar{U}_1^i + J^{i+1} (\bar{U}_1^i)_\eta \right) & \end{aligned} \quad (15)$$

Note that Eqs. (14) and (15) are in the form of Eq. (9). Finally, at the shock boundary the flow variables are initially assumed to be the same as the previous marching step (freestream conditions), i.e.

$$(J\bar{U})^{i+1} = (J\bar{U})^i$$

which implies

$$J^{i+1}\Delta\bar{U}^i = (J^i - J^{i+1})\bar{U}^i \quad (16)$$

At each station, the shock slope and the flow variables are iteratively corrected by using compatibility and Rankine-Hugoniot relations in an explicit manner. The iterative process is repeated at the shock until the solution converges, and then the solution marches on the next solution plane.

To have a tridiagonal system of equations, two two-point compact third-order schemes are used for the points adjacent to the wall and shock boundaries

$$\begin{aligned} f_j - f_{j+1} + (\Delta\eta)f'_j + \frac{(\Delta\eta)^2}{6}(2f''_j + f''_{j+1}) + O(\Delta\eta)^4 &= 0 \\ f_j - f_{j+1} + (\Delta\eta)f'_{j+1} + \frac{(\Delta\eta)^2}{6}(f''_j + 2f''_{j+1}) + O(\Delta\eta)^4 &= 0 \end{aligned} \quad (17)$$

The simplicity of treating boundary conditions of Von-Neumann type with the compact method is one of the advantages of using compact schemes that is worth mentioning here. The boundary finite difference schemes 17 allow applying boundary conditions, Eqs. (14) and (15), without missing the tridiagonality of the system of equations while preserving the third-order accuracy at the boundaries.

3.3 Block Tridiagonal System of Equations

The preceding system of Eqs. (9) and (10) along with the above boundary conditions forms a block tridiagonal system of equations for $\{X\} = \{\Delta\bar{U}^i, \Delta\bar{U}_\eta^i, \Delta\bar{U}_{\eta\eta}^i\}^T$ with a block size of 12×12 as follows:

$$[M]\{X\} = \{R\} \quad (18)$$

where

$$[M] = \begin{bmatrix} B_1 & D_1 & & & & \\ & \ddots & \ddots & \ddots & & \\ & & A_j & B_j & D_j & \\ & & & \ddots & \ddots & \ddots \\ & & & & A_{J_{\max}} & B_{J_{\max}} \end{bmatrix},$$

$$\{X\} = \begin{Bmatrix} X_1 \\ \vdots \\ X_j \\ \vdots \\ X_{J_{\max}} \end{Bmatrix}, \quad \{R\} = \begin{Bmatrix} R_1 \\ \vdots \\ R_j \\ \vdots \\ R_{J_{\max}} \end{Bmatrix}$$

where the block elements are

$$\begin{aligned} B_1 &= \begin{bmatrix} C_0 & C_1 & C_2 \\ I & hI & \frac{h^2I}{3} \\ I & O & -\frac{h^2I}{6} \end{bmatrix}, \\ D_1 &= \begin{bmatrix} O & O & O \\ -I & O & \frac{h^2I}{6} \\ -I & O & -\frac{h^2I}{6} \end{bmatrix}, \\ & j = 1 \\ A_j &= \begin{bmatrix} O & O & O \\ -I & -\frac{hI}{3} & O \\ I & O & -\frac{h^2I}{12} \end{bmatrix}, \\ B_j &= \begin{bmatrix} C_0 & C_1 & C_2 \\ O & -\frac{4hI}{3} & O \\ -2I & O & -\frac{10h^2I}{12} \end{bmatrix}, \\ D_j &= \begin{bmatrix} O & O & O \\ I & -\frac{hI}{3} & O \\ I & O & -\frac{h^2I}{12} \end{bmatrix}, \\ & 2 \leq j \leq J_{\max} - 1 \\ A_{J_{\max}} &= \begin{bmatrix} O & O & O \\ -I & -hI & -\frac{hI}{3} \\ -I & O & \frac{h^2I}{6} \end{bmatrix}, \\ B_{J_{\max}} &= \begin{bmatrix} C_0 & C_1 & C_2 \\ I & O & -\frac{h^2I}{6} \\ I & -hI & \frac{h^2I}{3} \end{bmatrix}, \\ & j = J_{\max} \end{aligned}$$

and the unknown and right-hand side vectors are

$$X_j = \begin{Bmatrix} \Delta U \\ \Delta U_\eta \\ \Delta U_{\eta\eta} \end{Bmatrix}, \quad X_j = \begin{Bmatrix} C_R \\ O \\ O \end{Bmatrix}$$

where I is a 4×4 identity matrix and O is a 4×4 zero matrix or zero vector of length 4. The matrices C_0 , C_1 and C_2 introduce the governing equation 2 and also the boundary conditions into the system of equations.

A block-tridiagonal solver is used to calculate the incremental solution vector $\{X\} = \{\Delta\bar{U}^i, \Delta\bar{U}_\eta^i, \Delta\bar{U}_{\eta\eta}^i\}^T$, and then the flow variables and the first and second derivatives are automatically determined as follows

$$\begin{aligned}\bar{U}^{i+1} &= \bar{U}^i + \Delta\bar{U}^i \\ \bar{U}_\eta^{i+1} &= \bar{U}_\eta^i + \Delta\bar{U}_\eta^i \\ \bar{U}_{\eta\eta}^{i+1} &= \bar{U}_{\eta\eta}^i + \Delta\bar{U}_{\eta\eta}^i\end{aligned}\quad (19)$$

3.4 Solution of IPNS Equations

As mentioned before, for computing the flowfield using the single sweep PNS scheme, the explicit streamwise pressure gradient term ΔP^i in Eq. (8) is dropped. For the solution of the IPNS model, the above algorithm can be used and the streamwise pressure gradient term is treated by employing the ADE procedure. The ADE method, using a first-order forward difference formula for the explicit pressure gradient term in Eq. (6), is written in two steps as follows:

First step:

$$\begin{aligned}\left. \frac{\partial p}{\partial \xi} \right|^{i+1} &= \omega \frac{p_m^{i+1} - p_m^i}{\Delta \xi} + \\ (1 - \omega) \left[\frac{p_k^{i+1} - p_k^i}{\Delta \xi} - \frac{p_m^{i+1} - p_k^{i+1}}{\Delta t} \right]\end{aligned}\quad (20)$$

In this step, the PNS equations are solved with the streamwise pressure gradient given by Eq. (20). The solution is marched from the upstream to the downstream boundary to obtain the pressure distribution at the intermediate time level p_m .

Second step:

$$\begin{aligned}\frac{p_k^{i+2} - p_k^{i+1}}{\Delta \xi} - \frac{p_m^{i+1} - p_k^{i+1}}{\Delta t} &= \\ \frac{p_{k+1}^{i+2} - p_{k+1}^{i+1}}{\Delta \xi} + \frac{p_{k+1}^{i+1} - p_m^{i+1}}{\Delta t}\end{aligned}\quad (21)$$

The above equation is solved by marching the solution from the downstream to the upstream boundary to obtain the pressure at the new time level p_{k+1} . This simple relation enforces the propagation of information upstream in a relatively rapid manner.

An appropriate outflow boundary condition for the IPNS solution is provided by setting the streamwise pressure gradient equal to zero at the outer boundary. The IPNS solution requires the initial pressure distribution in the subsonic region. The initial guess can be adequately provided by solving the standard single sweep PNS model. As this initial condition is provided, the solution of the IPNS model is obtained by the ADE procedure, and the pressure is stored at all stations only in the subsonic region. Then, the process is repeated until the solution converges to a specified convergence criterion. To accelerate the convergence rate of the IPNS model, the under-relaxation procedure for pressure calculation in the subsonic region is applied as follows:

$$p_{k+1} = \Omega_p p_{k+1} + (1 - \Omega_p) p_k, \quad \Omega_p < 1 \quad (22)$$

4 Numerical Results

The high-order accurate solution of hypersonic axisymmetric flows is obtained by implementing the fourth-order compact finite-difference method to the PNS and globally iterated PNS (IPNS) equations. At first, the dispersive and dissipative properties of the compact method are studied. Then, the fourth-order compact method is implemented to the quasi one-dimensional Euler equations to solve compressible flow inside the Shubin nozzle. Finally, The numerical solutions of the fourth-order compact PNS and IPNS schemes are presented for hypersonic flow over a blunt cone at Mach 8. A sensitivity study is also performed to investigate the effects of grid size and numerical dissipation term on the accuracy of basic flow profiles and their derivatives.

Table 1 Stability bound of different space and time discretization for the linear wave equation where $r = c\Delta t/\Delta x$ is the courant number.

Space Discretization	Time Discretization	Stability Bound
Central 4th-order	Forward	$r = 0$
	Central	$r = 0$
	Backward	$r \in \mathfrak{R}$
Forward 3rd-order	Forward	$r = 0$
	Central	$r \in \mathfrak{R}^-$
	Backward	$r \in \mathfrak{R} - (0, \frac{1}{3})$
Backward 3rd-order	Forward	$r = 0$
	Central	$r \in \mathfrak{R}^+$
	Backward	$r \in \mathfrak{R} - (\frac{-1}{3}, 0)$

4.1 Numerical Stability Analysis of Compact Schemes

The central fourth-order and upwind third-order compact schemes are first examined by solving the one-dimensional linear wave equation, that is, $u_t + cu_x = 0$. The purpose of this task is to confirm the numerical stability of the schemes. Furthermore, the modified differential equations for several time discretization schemes and also amplitude and phase errors of each of them are derived to study dispersive and dissipative properties of the methods. Table 1 shows the stability bound of different schemes. The results show that forward time-differencing is unconditionally unstable and backward time-differencing is unconditionally stable for the central compact scheme for the linear wave equation.

4.2 One-Dimensional Nozzle Flow

Since the Navier-Stokes equations have nonlinear terms which may lead to instability, before applying the compact method to the parabolized Navier-Stokes (PNS) equations, the fourth-order compact scheme is applied to the quasi one-dimensional Euler equations for computing compressible flow inside the Shubin nozzle [7, 14] to gain some numerical experiences. A 6th-order dissipation term is used to stabilize the numerical instability of the scheme. The flow is supersonic and the characteristic boundary conditions are used at the outlet. Figure 2 shows the non-dimensional pressure distribution along the nozzle.

Table 2 Comparison of computed and exact pressure values at middle of the nozzle ($x = 5$) for $\epsilon_n = 0.001$.

Δx	Computed value	Error
1.0	0.5413949558016263	$0.4940560582674669E-03$
0.5	0.5418449196455760	$0.4409221431778132E-04$
0.25	0.5418861898342086	$0.2822025685245144E-05$
0.125	0.5418887835033724	$0.2283565213589966E-06$
Exact	0.5418890022432340	—————

zle using 20 grid points, while Table 2 gives the value of non-dimensional pressure in the middle of the nozzle ($x = 5$) and the corresponding error for different grid spacing. The fourth-order accuracy of the method is demonstrated by comparison with the exact solution, as shown in Fig. 3.

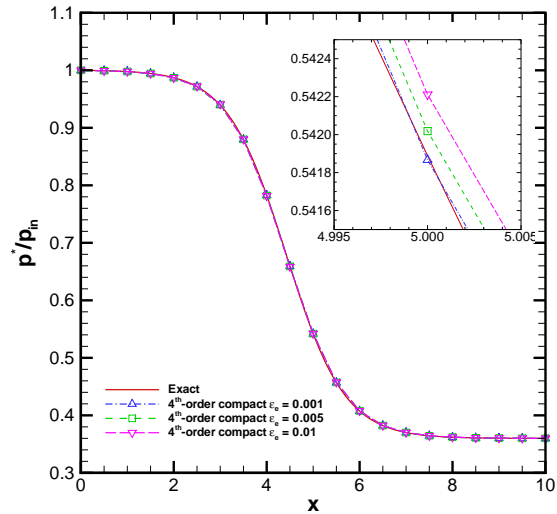


Fig. 2 Comparison of computed and exact pressure distributions along the nozzle.

4.3 Hypersonic Flow over a Blunt Cone

The numerical solution of the parabolized Navier-Stokes (PNS) equations for computing supersonic/hypersonic flowfields is carried out by using the fourth-order compact finite-difference method. Both the PNS and globally iterated PNS (IPNS) models are used. The geometry and the freestream conditions are adapted to the wind-tunnel blunt cone experiment of Stetson et al [15]. For this blunt cone, the flow condi-

Implementation of High-Order Compact schemes to the Iterative Parabolized Navier-Stokes Equations

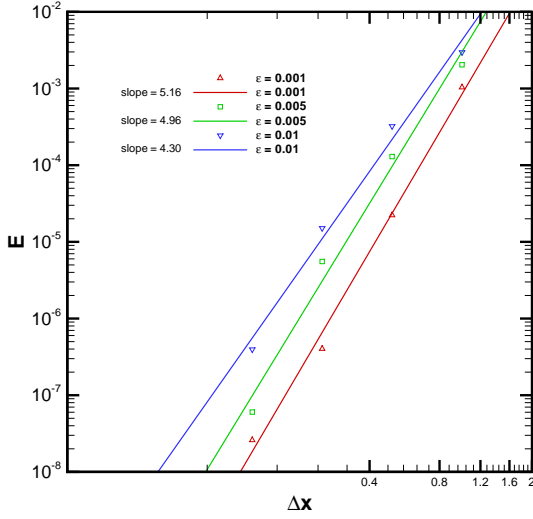


Fig. 3 Order analysis of numerical solution of the Shubin nozzle by the 4th-order compact method. Symbols indicate numerical values and solid lines indicate power-fitted curves.

tions are a freestream Mach number of $M_\infty = 8$, a freestream unit Reynolds number of $Re_\infty/m = 8.2021 \times 10^6$ and a freestream temperature of $T_\infty^* = 54.3\text{K}$ (the starred variables are referred to dimensional ones). The blunt cone has a half-angle of $\theta_c = 7^\circ$, and the study is performed at zero angle of attack. The blunt cone has a spherical nose radius of $R_N = 3.81\text{mm}$, and the freestream Reynolds number based on this length is $Re_\infty = 31250$. For this case, a sensitivity study is performed for the basic state solution, including the profiles and their derivatives obtained from the high-order compact PNS and IPNS schemes, and the effects of grid size and numerical dissipation term used are discussed. All profiles and their derivatives calculated by the fourth-order compact PNS and IPNS models are presented at the marching station, $S^*/R_N = 175$.

The second-order central TLNS code [5, 12] solves the subsonic region of the flowfield up to $S = S^*/R_N \leq 4.0$ with 80 grid points in the streamwise direction and 100, 200 and 400 grid points in the wall-normal direction to provide the initial data plane for the solution of the PNS and IPNS codes. The marching stepsize for the PNS

and IPNS codes, $\Delta\xi$, is chosen to be the same as that of the TLNS code, that is, $\Delta\xi = 0.05$. Figure 1 shows the regions solved by the TLNS and PNS equations. The present fourth-order compact PNS and IPNS codes have been thoroughly verified by comparison with those of the second-order method [3, 4]. Details of these investigations can be found in Refs. [3]-[7].

A grid independence study is conducted to evaluate the effects of grid size in the wall-normal direction on the flow variables. For this study, the Mach number profile is chosen due to its dependency on both the momentum and energy equations. Figure 4 compares the Mach number profile computed by the second-order central and fourth-order compact PNS models at the desired station, $S^*/R_N = 175$. The results of the second-order Beam and Warming method are performed for different grid points in the wall-normal direction. It is clear that $J_{\max} = 200$ is an adequate grid for the second-order method [3, 4]. It can be seen that the results of the fourth-order compact solution using $J_{\max} = 100$ are comparable with those of second-order solutions using $J_{\max} = 200$ and 400.

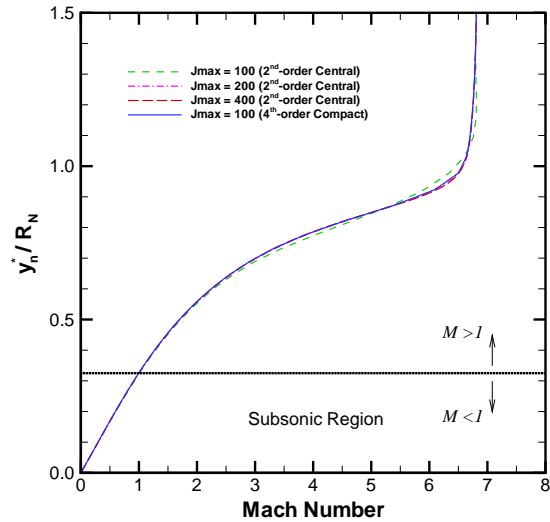


Fig. 4 Comparison of Mach number profile for the 2nd-order central and 4th-order compact PNS models for the blunt cone, $M_\infty = 8$ and $Re_\infty = 31250$ at $S = 175$.

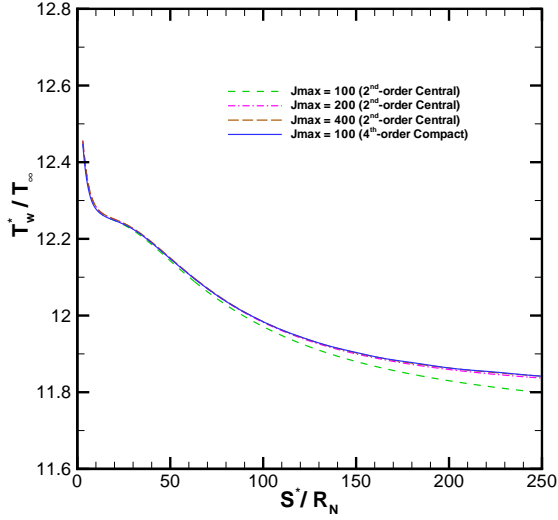


Fig. 5 Comparison of surface temperature distribution for the 2nd-order central and 4th-order compact PNS models for the blunt cone, $M_\infty = 8$ and $Re_\infty = 31250$.

Figure 5 presents a comparison of the surface temperature distribution for the second-order central and fourth-order compact PNS models for different number of grid points in the wall-normal direction. The compact method with $J_{max} = 100$ gives the same distribution as the second-order method with $J_{max} = 400$. The effect of numerical dissipation value in the compact solution of the PNS model on the surface temperature using $J_{max} = 100$ is examined in Fig. 6. No considerable difference is observed for the 6th-order dissipation, while the 4th-order dissipation significantly affects the surface temperature. The reason is that the numerical value of the 6th-order dissipation near the wall is much smaller than that of the 4th-order dissipation, with the same dissipation coefficient. The 4th-order dissipation term was also found to have significant effects on the surface temperature for the second-order method [3, 4].

To verify the order of a numerical method in a specific problem, it is usual to compare the value of variables in the interior nodes among different grid sizes. However, in this simulation due to dependency of the shock position to the numeri-

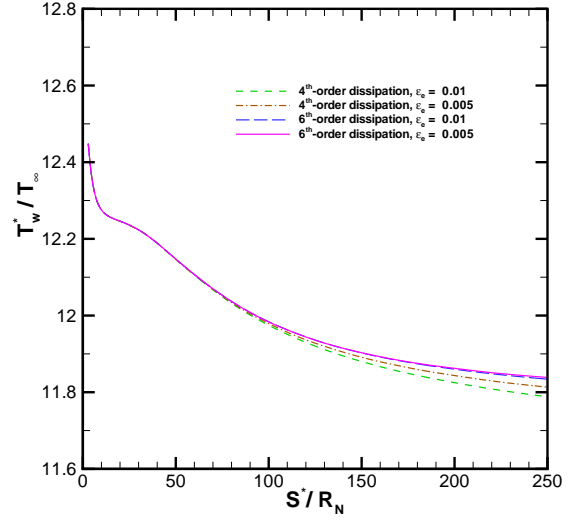


Fig. 6 Effect of 6th- and 4th-order dissipation terms on surface temperature distribution for the 4th-order compact PNS model for the blunt cone, $M_\infty = 8$ and $Re_\infty = 31250$.

cal solution and also due to nonuniformity of the grid, the position of the shock and consequently the position of the grid points in the wall-normal direction do not have the same location for different number of grid points. Due to this difficulty, one should select the surface variables for evaluating the accuracy of the method. However, the accuracy of the method is influenced by the boundary treatment used which is a third-order compact finite-difference scheme with respect to the first derivatives. For this study, the skin friction coefficient due to its dependency on the first derivative of the velocity is chosen to evaluate the numerical accuracy of the compact method. Three cases are considered for this analysis, that are, $J_{max} = 100, 200$ and 400 where the finest grid is considered to be the exact solution. To avoid local effects, the following L_2 -norm is defined

$$e = \left(\int_{S_1}^{S_2} |\psi - \psi_{exact}|^2 dS \right)^{\frac{1}{2}}, \quad \psi = C_f \quad (23)$$

where S_1 is taken far enough to remove the effect of initial conditions. Using the above norm,

the computed order of the compact method is obtained as

$$\log_2 \left(\frac{e_{100}}{e_{200}} \right) = 2.84$$

using

$$S_1 = 100, \quad S_2 = 200$$

which seems reasonable considering the boundary treatment used is third-order. However, the above value is observed to be dependent on S_1 , S_2 and the chosen variable and varies between 2.5 – 3.5. Beside accurate computation of the ba-

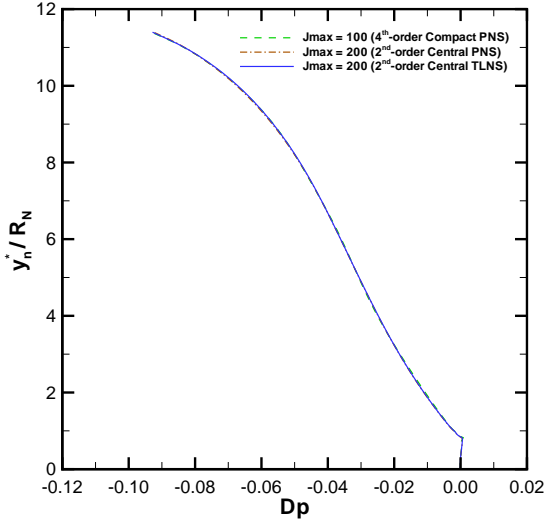


Fig. 7 Comparison of first derivative of pressure profile for the 2nd-order central and 4th-order compact PNS models and the TLNS model for the blunt cone, $M_\infty = 8$ and $Re_\infty = 31250$ at $S = 175$.

sic flowfield, the accuracy of the first and second derivatives of the flow variables with respect to the wall-normal direction are crucial for the flow stability analysis of high speed flows. In addition to the global accuracy, the main advantage of the present compact formulation for computing the flowfield is that the basic flow variables and their first and second derivatives are automatically calculated with the fourth-order accuracy and no intermediate computation of the derivatives, which usually produces oscillations in these profiles, is

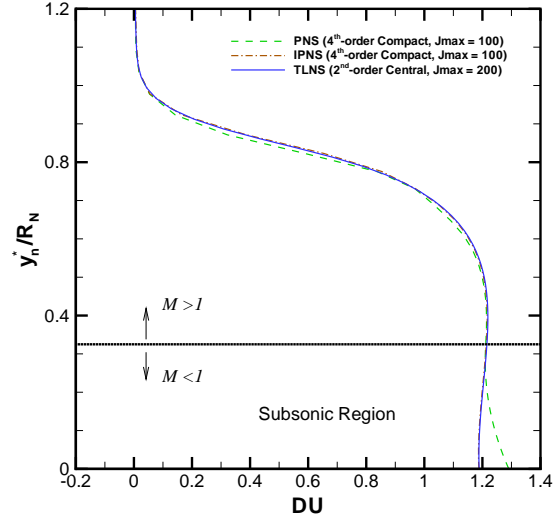


Fig. 8 Comparison of first derivative of velocity profile for the 4th-order compact PNS and IPNS models and the TLNS model for the blunt cone, $M_\infty = 8$ and $Re_\infty = 31250$ at $S = 175$.

required. Hereinafter, the symbol D represents the derivative with respect to the wall-normal direction $y_n = y_n^*/R_N$. Figure 7 shows the first derivative of the pressure profile Dp from the fourth-order compact PNS model using $J_{\max} = 100$ with those of the second-order PNS and TLNS models using $J_{\max} = 200$ at station 175 which shows no considerable difference among these curves. Note that the basic flow based on the TLNS model [5, 12] for the blunt cone studied herein are available for $J_{\max} = 200$ and $\bar{\beta} = 1.01$. Figure 8 shows a comparison of the first derivative of the streamwise velocity profile DU ($U = (u\xi_x + v\xi_y)/\sqrt{\xi_x^2 + \xi_y^2}$) from the fourth-order compact PNS and IPNS models using $J_{\max} = 100$ with those of the second-order TLNS model using $J_{\max} = 200$ at the desired station. The deviation of the PNS model is due to neglecting the explicit part of the streamwise pressure gradient in Eq. (2) which is not omitted in the IPNS model, and therefore, this deviation is completely compensated by the IPNS model. Although the results of the flowfield based on the IPNS and TLNS models are nearly the same,

the IPNS model is computationally more efficient than the TLNS model. Thus, using the fourth-order compact IPNS scheme, a high-order accurate and efficient basic flow model can be provided. Figure 9 compares the first derivative of the streamwise velocity profile DU from the IPNS model for the second-order central and fourth-order compact solutions. It is obvious that the results of the compact method with $J_{max} = 100$ is comparable with those of the second-order method using $J_{max} = 400$.

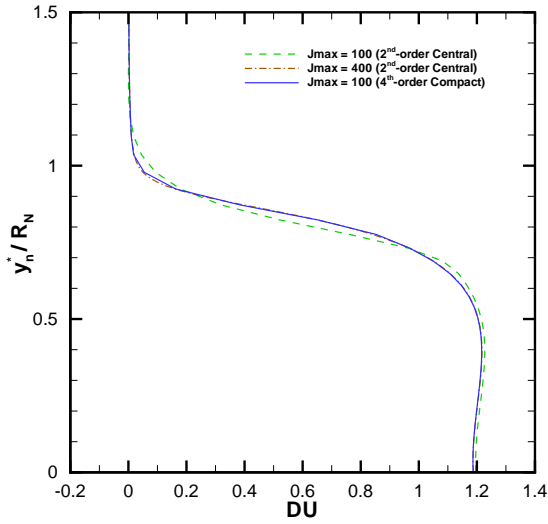


Fig. 9 Comparison of first derivative of velocity profile for the 2nd-order central and 4th-order compact IPNS models for the blunt cone, $M_\infty = 8$ and $Re_\infty = 31250$ at $S = 175$.

A sensitivity study is also performed for the higher derivatives of the flow variables. Figure 10 demonstrates the effect of grid refinement in the streamwise direction on the second derivative of the temperature profile, D^2T , computed by the fourth-order compact PNS model using $J_{max} = 200$ for different values of the marching stepsize $\Delta\xi$ at station 175. The figure shows marching stepsize does not affect on the D^2T profile. This is evident from the fact that the evolution of the flow in the streamwise direction at the afterbody region ($S \geq 75$) is very slow. To examine the improvement in the second derivatives of the flow variables, the profiles of D^2T for

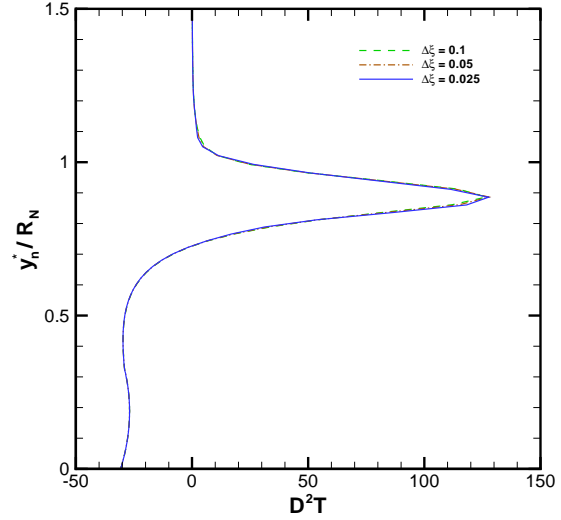


Fig. 10 Effect of grid refinement in the streamwise direction for second derivative of temperature profile in the 4th-order compact PNS solution for the blunt-cone, $M_\infty = 8$ and $Re_\infty = 31250$ at $S = 175$.

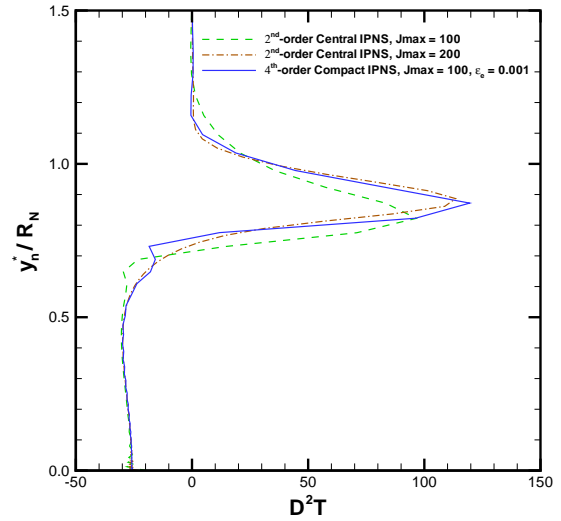


Fig. 11 Comparison of second derivative of temperature profile for the 2nd-order central and 4th-order compact IPNS models for the blunt cone, $M_\infty = 8$ and $Re_\infty = 31250$ at $S = 175$.

the second-order central and fourth-order compact IPNS models are shown in Fig. 11. The results of $J_{max} = 100$ for the compact method and

those of $J_{\max} = 200$ for the second-order method are nearly the same except in an oscillation near $y_n \approx 0.7$ which is close to high gradient region of the profile (the critical layer region). This oscillation is caused by the 6th-order dissipation term used. Figure 12 shows the values of the fourth element of dissipation vector which correspond to the energy equation. As the grid becomes finer or a smaller dissipation value is used, the amount of dissipation becomes closer to zero. Figure 13 presents the effect of numerical dissipation on the second derivative of the temperature profile D^2T from the fourth-order compact IPNS model for different grids and different values of dissipation coefficient. It is clear that the oscillation in the second derivative of temperature profile can be eliminated by using a finer grid, i.e. $J_{\max} = 140$ or by choosing a smaller amount of dissipation value, i.e. in the range of $\varepsilon_e = 0.0002 - 0.0005$ instead of 0.001. For fine grids the value of ε_e can be in the range of $\varepsilon_e = 0.0001 - 0.001$ without any considerable effect in the results, however, for smaller values of dissipation, very small oscillations can be seen in the boundary layer region. It was found that in general for coarse grids, the dissipation term can influence higher derivatives of the flow variables. Therefore, special attention should be paid in using the artificial dissipation for stabilizing the numerical instability of high-order compact finite-difference schemes to obtain accurate basic flow models.

In Fig. 14 the second derivative of the temperature profile D^2T is obtained by differencing the temperature values of the solution of the fourth-order compact IPNS model in two ways: 2nd-order central differencing and 4th-order compact differencing. It shows the maximum value of D^2T in the critical region is predicted better with compact differencing, especially for a lower number of grid points i.e., $J_{\max} = 100$. As the number of grid points increases, the accuracy of the higher derivatives of the basic flow profiles becomes independent of the way of computing the derivatives.

Finally, the CPU-time comparison of the various solutions for the same case is performed to show the efficiency of using the high-order

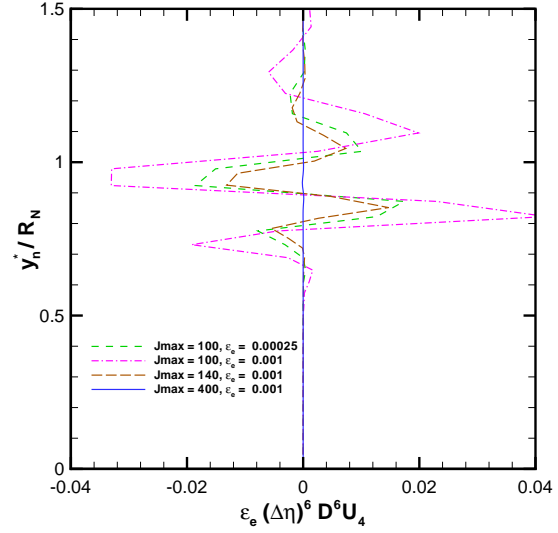


Fig. 12 Distribution of 6th-order dissipation term for different numerical dissipation and grid spacing in the 4th-order compact PNS solution for the blunt cone, $M_\infty = 8$ and $Re_\infty = 31250$ at $S = 175$.

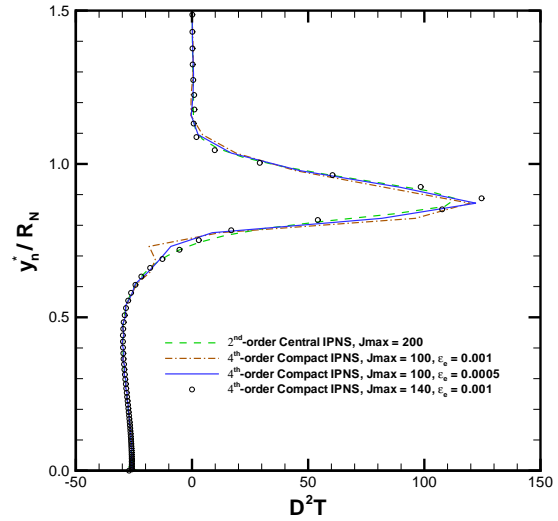


Fig. 13 Effect of numerical dissipation value and grid size on second derivative of temperature profile in the 4th-order compact IPNS solution for the blunt cone, $M_\infty = 8$ and $Re_\infty = 31250$ at $S = 175$.

compact PNS schemes. The present calculations using the PNS and IPNS schemes are performed on a 3.2-GHz Pentium IV computer. Fig-

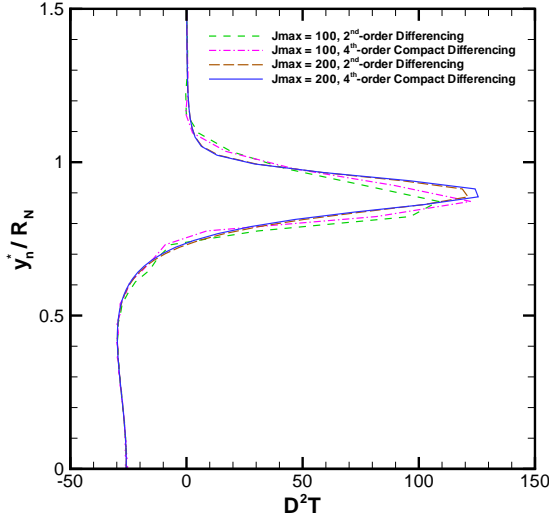


Fig. 14 Comparison of second derivative of temperature profile for the 2nd-order and 4th-order compact differencing of the compact IPNS solution for the blunt cone, $M_\infty = 8$ and $Re_\infty = 31250$ at $S = 175$.

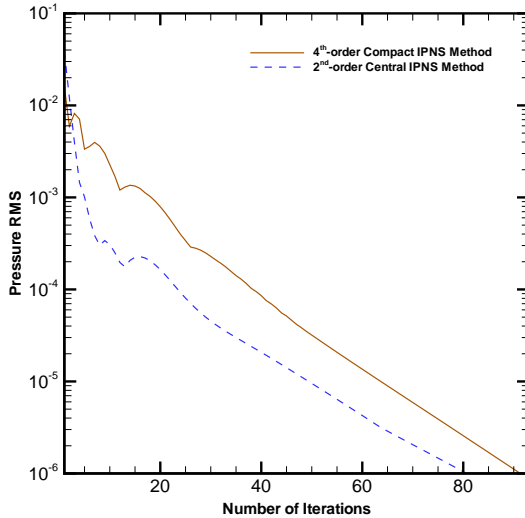


Fig. 15 Convergence history of the 2nd-order central and 4th-order compact IPNS models using $\Delta\xi/\Delta t = 0.4$ and $\Omega = 0.7$ for the blunt cone, $M_\infty = 8$ and $Re_\infty = 31250$.

ure 15 shows the convergence history of both the second-order central and fourth-order compact IPNS models using $\Delta t/\Delta\xi = 2.5$ and $\Omega = 0.7$ for the blunt cone studied herein. These solutions

are obtained with $J_{\max} = 200$ for the global region $4 \leq S \leq 250$ which includes approximately 5000 marching steps for each global iteration. The computations are considered to be converged when the root mean square (RMS) of the relative change in pressure is less than 1×10^6 . The numbers of global iterations for convergence of the second-order central and fourth-order compact IPNS models are about 81 and 92, respectively. The computation times are about 9 and 190 minutes for the second-order central and fourth-order compact IPNS models (6 and 120 seconds for those of the PNS models), respectively. The CPU time of the second-order TLNS solution for the region $S \leq 250$ using $J_{\max}=200$ grid points was about 260h on a Cray Y-MP [5, 12]. It is clear that both the fourth-order compact PNS and IPNS schemes are suitable for accurate and efficient computation of basic flow models in comparison with the TLNS scheme.

5 Conclusions

The numerical solution of the parabolized Navier-Stokes schemes for computing supersonic/hypersonic axisymmetric flowfields is obtained by using the fourth-order compact finite-difference method. Both the PNS and IPNS models are considered. Some significant conclusions regarding the present calculations based on the high-order compact PNS schemes are summarized as follows:

1. The present results indicate that surface variables are accurately computed by the compact method whereas the second order method shows considerable different results with different grid spacing. The compact method is capable of computing the flowfield variables especially their derivatives more accurately than the second-order method.
2. In addition to the global accuracy, the main benefit of using the present high-order compact formulation for the solution of the flowfield is that the derivatives of the flow variables, required for stability

computations, are automatically calculated with the same accuracy of the flow variables and no intermediate computation of the derivatives, which usually produces oscillations in these profiles, is needed. Note that treating the Von-Neumann boundary condition is much simpler with the compact method without loss of accuracy and tridiagonality.

3. It is demonstrated that the derivatives of the flowfield variables computed based on high-order compact methods are sensitive to the number of grid points and especially the numerical dissipation. Using the compact method no further clustering is needed near the wall and special attention should be focused on the critical layer. To obtain more accurate solution especially in the derivatives near the critical layer, high-order dissipation term with a reasonable coefficient must be added. The study indicates that any practical development in high-order compact methods requires a more sophisticated numerical dissipation.
4. Although the results of the flowfield based on the IPNS and TLNS models are almost identical, the IPNS model is computationally more efficient than the TLNS model. Therefore, using the fourth-order compact IPNS model, a high-order accurate and efficient basic flow model can be provided.
5. The present study introduces the high-order compact solutions of the PNS schemes for providing accurate and efficient basic flow models to be used for the stability analysis and transition prediction of hypersonic axisymmetric flows.

Acknowledgments

The authors would like to thank the University of Tehran and Sharif University of Technology for financial support of this project. Also the authors would thank assistant professor Sarmad

Ghader for his valuable comments on the compact schemes.

A Linear Stability of 6th-Order Dissipation Term

To obtain the stability bound for ϵ_e we consider the one-dimensional linear wave equation and the 6th-order dissipation term:

$$u_t + cu_x = \epsilon_e \frac{(\Delta x)^6}{(\Delta t)} u_{xxxxxx}$$

Now using the compact differencing for the space discretization and Euler implicit method for the time-marching scheme and also using the operator notation for the 6th-order dissipation, we have

$$\begin{aligned} u^{n+1} - u^n + rQ^{-1}Du^{n+1} &= \epsilon_e(\nabla\Delta)^3u^n \\ r &= \frac{c\Delta t}{\Delta x} \\ Qu_i &= \frac{u_{i+1} + 4u_i + u_{i-1}}{6} \\ Du_i &= \frac{u_{i+1} - u_{i-1}}{2} \\ (\nabla\Delta)u_i &= u_{i+1} - 2u_i + u_{i-1} \end{aligned}$$

and implementing the Von-Neumann stability analysis, the amplification factor will be

$$\begin{aligned} g &= \frac{\hat{u}^{n+1}}{\hat{u}^n} = \frac{(\epsilon_e(\nabla\Delta)^3 + 1)e^{jik_mx}}{(1 + rQ^{-1}D)e^{jik_mx}} \\ &= \frac{Q(\epsilon_e(\nabla\Delta)^3 + 1)e^{jik_mx}}{(Q + rD)e^{jik_mx}} \\ &= \frac{(\cos\beta + 2)(\epsilon_e(2\cos\beta - 2)^3 + 1)}{(\cos\beta + 2) + 3jr\sin\beta} \\ u_i^n &= \sum \hat{u}_i^n e^{jik_mx} \\ j &= \sqrt{-1}, \quad 0 < \beta = k_m\Delta x < \pi \end{aligned}$$

For the stability we require $|g| < 1$ and the maximum of the above function occurs at $\beta = \pi$, therefore the stability bound is

$$0 \leq \epsilon_e \leq \frac{1}{32} = 0.03125$$

References

- [1] Tolstykh, A. L., *High Accuracy Non-Centered Compact Difference Schemes for Fluid Dynamics Applications*, World Scientific, Singapore, 1994.
- [2] Lele, S.K. and Tatineni, M., "Compact finite difference schemes with Spectral-like Resolution," *Journal of Computational Physics*, Vol. 103, 1992, pp. 16, 42.
- [3] Esfahanian, V. and Hejranfar, K., "Accuracy of Parabolized Navier-Stokes Schemes for Stability Analysis of Hypersonic Axisymmetric Flows," *AIAA Journal*, Vol. 40, No. 7, 2002, pp. 1311-1322.
- [4] Hejranfar, K., "Computation and Stability Analysis of Hypersonic Axisymmetric Flows Using Parabolized Schemes," Ph.D. thesis, University of Tehran, March 2002.
- [5] Esfahanian, V., "Computation and Stability Analysis of Laminar Flow over a Blunted Cone in Hypersonic Flow," Ph.D. thesis, Ohio State University, Columbus, June 1991.
- [6] Esfahanian, V., Hejranfar, K. and Mahmoodi Darian, H., "Implementation of Compact Finite-Difference Method to Parabolized Navier-Stokes Equations," *The 13th Annual Conference of the Computational Fluid Dynamics Society of Canada*, CFD 2005, Newfoundland, Canada, 2005.
- [7] Mahmoodi, H., "Computation of Parabolized Navier-Stokes Equations Using Compact Finite-Difference Method," Ms. thesis, University of Tehran, Sept. 2004.
- [8] Tannehill, J. C., Anderson, D. A., and Pletcher, R. H., *Computational Fluid Mechanics and Heat Transfer*, 2nd ed., Taylor and Francis, Washington, DC, 1997.
- [9] Vigneron, Y. C., Rakich, J. V., and Tannehill, J. C., "Calculation of Supersonic Viscous Flow over Delta Wings with Sharp Subsonic Leading Edges," AIAA paper 78-1137, July 1978.
- [10] Schiff, L. B., and Steger, J. L., "Numerical Simulation of Steady Supersonic Viscous Flow," *AIAA Journal*, Vol. 18, No. 12, 1980, pp. 1421-1430.
- [11] Barnett, M., and Davis, R. T., "Calculation of Supersonic Flows with Strong Viscous-Inviscid Interaction," *AIAA Journal*, Vol. 24, No. 12, 1986, pp. 1949-1455.
- [12] Esfahanian, V., Herbert, Th., and Burggraf, O. R., "Computation of Laminar Flow over a Long Slender Axisymmetric Blunted Cone in Hypersonic Flow," AIAA Paper 92-0756, Jan. 1992.
- [13] Beam, R. M., and Warming, R. F., "An Implicit Factored scheme for the Compressible Navier-Stokes equations," *AIAA Journal*, Vol. 16, No. 4, 1978, pp. 393-402.
- [14] Shubin C. R., Stephens A. B. and Glaz H. M., Donaldson, "Steady Shock Tracking and Newton's Method Applied to One-Dimensional Duct Flow," *Journal of Computational Physics*, 1981, pp. 364-374.
- [15] Stetson, K. F., Thompson, E. R., Donaldson, J. C., and Siler, L. G., "Laminar Boundary Layer Stability Experiments on a Cone at Mach 8, Part 2: Blunt Cone," AIAA paper 84-0006, Jan. 1984.